Available online at www.sciencedirect.com
ScienceDirect
Journal of Magnetic Resonance 184 (2007) 29–38
JMR Journal of Magnetic Resonance
www.elsevier.com/locate/jmr

Use of multi-coil parallel-gap resonators for co-registration EPR/NMR imaging

Yuuki Kawada [a], Hiroshi Hirata [a,*], Hirodata Fujii [b]

[a] Department of Electrical Engineering, Yamagata University, Yonezawa, Yamagata 992-8510, Japan
[b] School of Health Sciences, Sapporo Medical University, Sapporo, Hokkaido 060-8556, Japan

Received 23 June 2006; revised 12 September 2006
Available online 6 October 2006

Abstract

This article reports experimental investigations on the use of RF resonators for continuous-wave electron paramagnetic resonance (cw-EPR) and proton nuclear magnetic resonance (NMR) imaging. We developed a composite resonator system with multi-coil parallel-gap resonators for co-registration EPR/NMR imaging. The resonance frequencies of each resonator were 21.8 MHz for NMR and 670 MHz for EPR. A smaller resonator (22 mm in diameter) for use in EPR was placed coaxially in a larger resonator (40 mm in diameter) for use in NMR. RF magnetic fields in the composite resonator system were visualized by measuring a homogeneous 4-hydroxy-2,2,6,6-tetramethyl-piperidinooxy (4-hydroxy-TEMPO) solution in a test tube. A phantom of five tubes containing distilled water and 4-hydroxy-TEMPO solution was also measured to demonstrate the potential usefulness of this composite resonator system in biomedical science. An image of unpaired electrons was obtained for 4-hydroxy-TEMPO in three tubes, and was successfully mapped on the proton image for five tubes. Technical problems in the implementation of a composite resonator system are discussed with regard to co-registration EPR/NMR imaging for animal experiments.

Keywords: Co-registration imaging; EPR/NMR imaging; Resonator; Implementation

1. Introduction

Non-invasive imaging techniques are important advancements in clinical and biomedical studies. For example, proton magnetic resonance imaging (MRI) can provide anatomical images of human bodies. Electron paramagnetic resonance (EPR) spectroscopy is also a magnetic resonance technique that can be used to detect specific molecules with unpaired electrons, i.e., free radicals. While electron paramagnetic resonance imaging (EPRI) techniques can show the spatial distributions of free radicals in a subject animal, a lack of anatomical images is a technical problem in determining the distribution of free radicals in an animal's organs. If an EPR image of free radicals is superimposed on an anatomical image obtained with MRI, it could be very useful for identifying the distributions of free radicals in the organs of a subject animal. Such a multimodal imaging method is urgently needed in biomedical sciences. There are two ways to map the images of free radicals on an anatomical image of a subject. One is to use a combination of proton-MRI and EPRI [1–3], and the other is to use Overhauser-enhanced magnetic resonance imaging (OMRI), also called proton–electron double resonance imaging (PEDRI) [4–7]. These imaging modalities can address the technical problem of EPRI regarding a lack of anatomical images.

The unification of proton-MRI and EPRI, called co-registration electron paramagnetic resonance/nuclear magnetic resonance (EPR/NMR) imaging, requires technological advances in magnets, RF coils, and software [8,9]. Sato et al. [1] reported their EPR/NMR imaging instrument. They used 680-MHz cw-EPR and 27.7-MHz cw-NMR spectrometers to obtain EPR/NMR images.

* Corresponding author. Fax: +81 238 26 3299.
E-mail address: hhirata@yz.yamagata-u.ac.jp (H. Hirata).

1090-7807/$ - see front matter © 2006 Elsevier Inc. All rights reserved.
doi:10.1016/j.jmr.2006.09.014

Some of the RF components in the EPR/NMR spectrometers were the same, such as an RF resonator, an electromagnet, a VSWR bridge, and an RF signal source. In this instrument, a loop-gap resonator with a transmission line was used for MRI at 27.7 MHz and EPRI at 680 MHz. The resonator was enclosed with a shielding case that had been used for an EPR instrument. A bulky shielding case is problematic for use in a pulsed MRI scanner, since the magnetic field gradient changes with a fast raise-time in data-acquisition processes. Thicker conductive elements disturb a time-varying magnetic field gradient due to eddy currents in the conductive elements. Since several pulse sequences are very beneficial for MRI experiments, RF resonators and shielding cases used in EPR/NMR imaging have to be compatible with modern pulsed MRI scanners.

In addition to the report by Sato and his colleagues, individual instruments (EPRI and MRI) have been used for co-registration EPR/NMR imaging. Matsumoto et al. [3] reported a composite resonator system that was used for a clinical 0.2-T MRI scanner and a 300-MHz cw-EPR imager. In this resonator system, irradiation and detection coils (8.5 MHz) and a parallel coil resonator (300 MHz) were combined to perform co-registration EPR/NMR imaging. In MRI, the irradiation coil was a saddle coil 535 mm in diameter and 780 mm in length. The detection coil was a solenoid coil 60 mm in diameter and 40 mm in length. Clinical MRI scanners are superior for measuring human bodies, but are not necessarily suitable for use in small animals. A resonator system that is fit for small-animal imaging would be useful for co-registration EPR/NMR imaging in small rodents. We focused on a composite resonator system for small-animal imaging. Such a resonator system would have to be suitable for the magnets used in an MRI scanner and an EPR imager.

There is another approach for making co-registration EPR/NMR imaging possible; a subject animal is transferred between EPRI and MRI instruments with a specially developed animal holder [2]. This holder avoids the misalignment of a subject animal in both EPRI and MRI instruments. Position markers are also used to adjust the registration of free radicals and proton images. The use of markers is a straightforward approach to make co-registration EPR/NMR imaging possible. It has been pointed out that a major limiting factor in the accuracy of image registration is the EPR image resolution. If spin probes with a broad absorption linewidth, e.g., nitroxide radicals, are used in experiments, the accuracy of the registration is limited due to the lower spatial resolution of EPRI.

This article describes investigations on the application of RF resonators for use in 0.5-T proton-MRI (21 MHz) and 24-mT cw-EPRI (670 MHz). These RF resonators were intended to measure the head of a mouse. We tested this composite resonator system with a capillary phantom, and demonstrated co-registration EPR/NMR imaging.

2. Methods

2.1. Design strategy

There are several requirements for a composite resonator system for co-registration EPR/NMR imaging: (i) the subject should be measured without any movement between the EPR and NMR resonators [10,11], (ii) each resonator should show good penetration of magnetic field modulation, and (iii) electromagnetic shielding for EPR should not interfere with time-varying magnetic field gradients in MRI pulse sequences. In addition to these general considerations, we had specific requirements for the resonators: (iv) the resonator system should have an appropriate sample-space for a mouse's head, (v) the resonance frequencies for NMR and EPR have to be compatible in our MRI scanner (21.8 MHz) and cw-EPR imager (600–700 MHz), and (vi) the dimensions of the resonator system should be suitable for the gap in the magnet used in EPR (55 mm). Since a 0.5-T MRI scanner has a wider gap (60 mm), our composite resonator system should fit within the narrower limit (55 mm).

To realize requirement (i), we aligned two resonators coaxially. This allowed us to measure a subject animal for both EPRI and MRI. For requirement (ii), we used a multi-coil, parallel-gap resonator for both imaging modalities. This resonator has less of a shielding effect for magnetic field modulation, compared to a conventional loop-gap resonator (LGR). The details of the multi-coil parallel-gap resonator (MCPGR) are described below. For requirement (iii), we used a thin-copper layer for part of a shielding case, which is helpful for reducing electromagnetic loss of the resonator due to radiation into the laboratory space. While a thin-copper layer (16 μm thick) works for electromagnetic shielding at the frequency used for EPR detection, it was intended to give less interference with a time-varying magnetic field gradient. We set the sample space for a mouse's head to be 18 mm in diameter, and the resonance frequencies for the two resonators were intended to be tuned to 21.8 and 650 MHz. The width of the shielding case was set to 54 mm.

2.2. Application of resonators

Fig. 1A shows a schematic of an MCPGR. While an MCPGR looks like a parallel coil resonator [3,12,13], it is electrically equivalent to a conventional LGR, as shown in Fig. 1B [14,15]. Five individual loops made of copper wire (1 mm thick) were soldered to a parallel-plate capacitor (0.79 mm thick) made of CuFlon® (CF-A-31-7-7, Polyflon Company, NY). To decrease the resonance frequency of the MCPGR used in NMR to 21.8 MHz, additional capacitors of 1.2 nF were connected to a parallel-plate capacitor. The inner diameter of the MCPGR used in NMR was 40 mm, and that of the MCPGR used in EPR was 22 mm. A Helmholtz coil pair (68 mm in mean diameter) for magnetic field modulation was placed on the wall

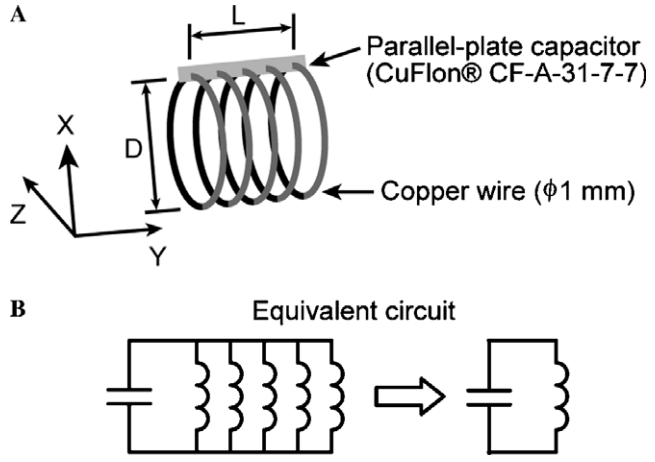

Fig. 1. (A) Schematic of a multi-coil parallel-gap resonator (MCPGR) for use in co-registration EPR/NMR imaging. The diameter D and axial length L of the MCPGR for NMR were 40 and 24 mm, respectively. The diameter D and axial length L of the MCPGR for EPR were 22 and 18 mm, respectively. The parallel-plate capacitors measured 5×23 mm (EPR) and 5×35 mm (NMR). The static magnetic field B_0 is perpendicular to the axis of the MCPGR. (B) Equivalent electrical circuit for the MCPGR.

of the shielding case. The modulation coil was used only for cw-EPR measurements, and could generate field modulation (90 kHz) up to 0.2 $mT_{p\text{-}p}$ with a high-speed amplifier (Model 4015, NF Corp., Japan). For both resonators, capacitive coupling was used to achieve good impedance matching (Figs. 2A and B). Non-magnetic trimmer capacitors (NMAJ55HV for use in NMR, NMAM25HV for use in EPR; Voltronics Corporation, NJ) were used for the matching circuits.

As illustrated in Fig. 3, two resonators were aligned coaxially to accommodate a subject up to 18 mm in diameter. Both resonators were mechanically supported by hollow bobbins made of Rexolite® 1422. The electromagnetic shielding for the MCPGR used in EPR should not interfere with the time-varying magnetic field gradient for MRI. To satisfy this requirement, we used a commercially available printed circuit board (FR-4, Sanhayato Corp., Japan) for the walls of the shielding case that are perpendicular to the static magnetic field. This board was made of epoxy resin with a fiberglass base. One side of the board had been laminated to a copper layer (16 μm thick). This copper layer is thick enough to shield electromagnetic waves at 670 MHz, since the skin depth at this frequency is only 2.6 μm in copper. In contrast, this leads to low eddy currents in the copper layer for the time-varying magnetic field in MRI.

Fig. 4A shows a photograph of the resonator system used in our experiments. There are two coaxial connectors that are input ports for the matching circuits of the MCPGRs. Fig. 4B also shows a photograph of the internal configuration of the resonator system. While the MCPGR for NMR is shown, the internal MCPGR for EPR is not shown in this photograph. The matching circuit for the MCPGR used for EPR was located on the upper plate,

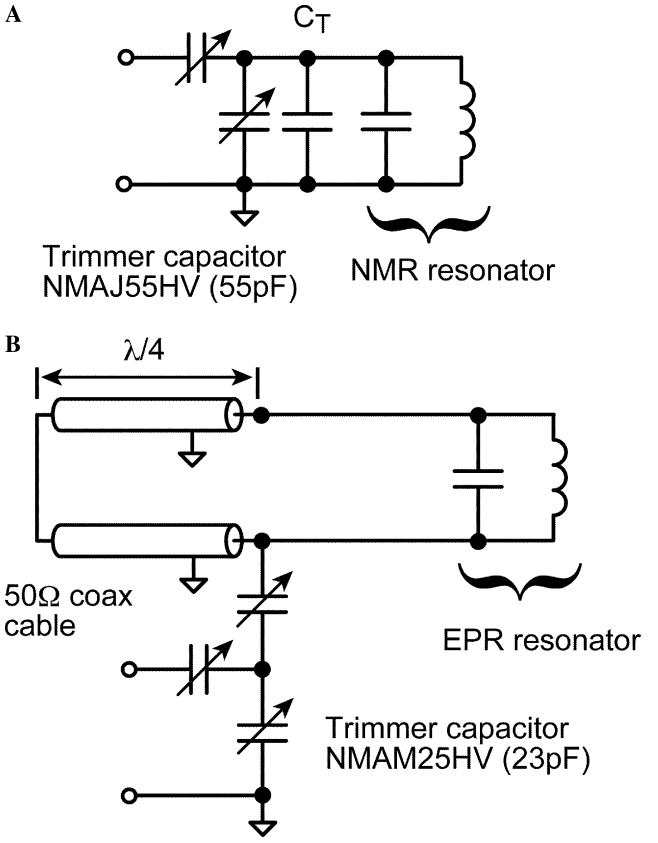

Fig. 2. (A) Matching network for the MCPGR used in NMR. A capacitor C_T, 1.2 nF, was added to the parallel-plate capacitor to adjust the resonance frequency to 21.8 MHz. (B) Matching network for the MCPGR used in EPR.

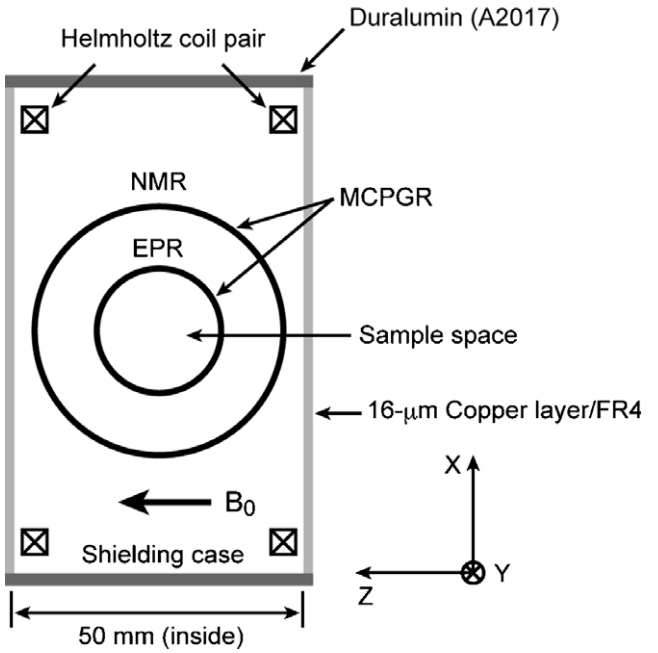

Fig. 3. Schematic cross-section of a composite resonator system. The MCPGR used in EPR was inserted into another MCPGR used in NMR. Hollow bobbins that support the MCPGRs are not shown. A Helmholtz coil pair was located in a shielding case and fixed to the sidewalls of the case. The sidewalls of the shielding case were made of epoxy resin on a fiberglass base and a 16-μm layer of copper.

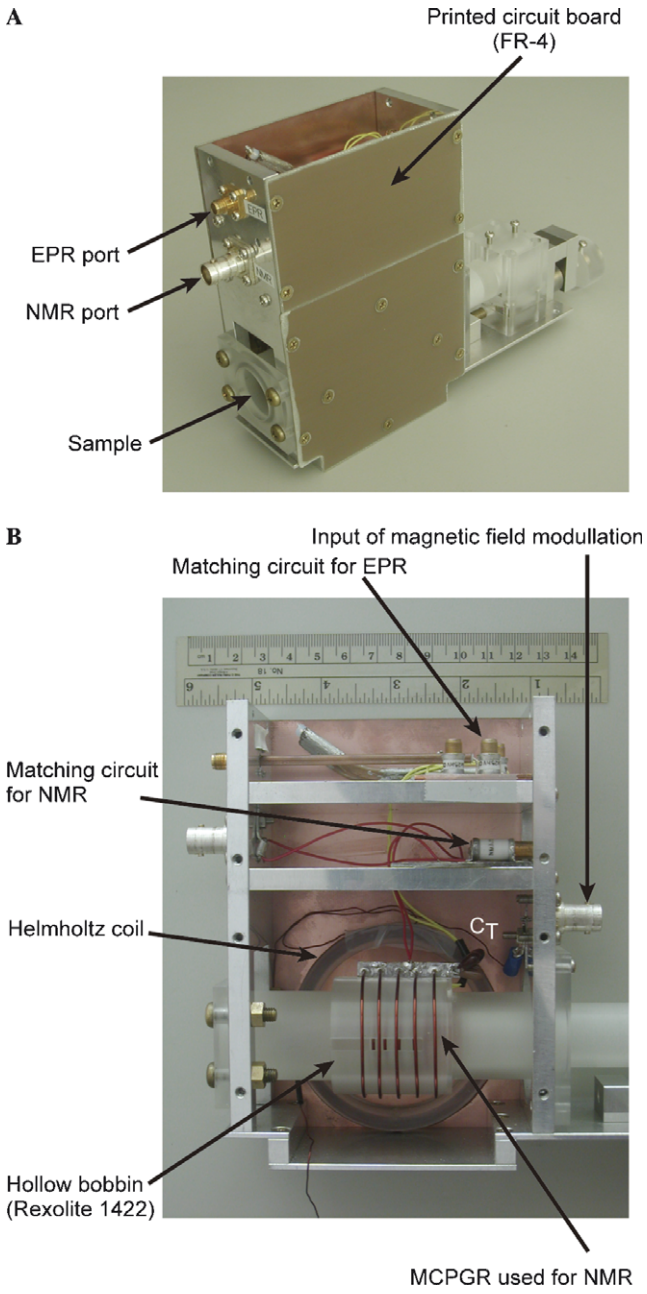

Fig. 4. (A) Photograph of the developed composite resonator system, and (B) its internal configuration.

and the matching circuit for the MCPGR for NMR was below that used for EPR. Additional capacitors (C_T) are visible near the parallel-plate capacitor. The shielding case has two openings. One was used to insert a subject, and the other was used to insert a hollow bobbin from the outside of the shielding case. Although this bobbin can be used to support a coupling loop for the MCPGR for EPR, we did not use the coupling loop in these experiments.

2.3. Phantom

We used two types of phantom in the experiments. For the first phantom, a test tube containing 5 mM 4-hydroxy-2,2,6,6-tetramethyl-piperidinooxy (4-hydroxy-TEMPO) solution was used to measure the distributions of image intensity for the MCPGRs. The test tube had an inner diameter of 14 mm and a length of 120 mm. Since the outer diameter of the test tube was 16 mm, the tube was wrapped with a thin Teflon sheet to keep it at the center of the MCPGRs. In the second phantom, five capillary tubes were used to demonstrate co-registration EPR/NMR imaging. The glass tubes (2.4 mm i.d.) contained distilled water, and, respectively, 2.5, 5, and 10 mM 4-hydroxy-TEMPO solution. These tubes were held with a bobbin (18 mm in diameter) made of Rexolite® 1422, and placed in the center of the MCPGRs. While distilled water is EPR-silent, 4-hydroxy-TEMPO solution is visible in EPRI.

2.4. EPR imager and MRI scanner

The implemented MCPGRs were tested with a home-built cw-EPR imager (24 mT) at Yamagata University and a 0.5-T proton-MRI scanner for small animals at Sapporo Medical University. The cw-EPR imager used an air-core Helmholtz coil and gradient coils that generated a magnetic field gradient in orthogonal directions. Image reconstruction code for two-dimensional (2D) EPRI was based on the direct Fourier transform reconstruction (DFTR) method. The imager and image reconstruction have been described elsewhere [16]. The parameters for cw-EPRI with the five capillary tubes were as follows: applied microwave power 7.6 dBm (5.8 mW), magnetic field scanning 8 mT, field gradient 50 mT/m, field modulation 0.15 mT, scan time 50 s, number of projections 64, total acquisition time 53 min, and time constant of the lock-in amplifier 100 ms. The field-of-view (FOV) was set to 160 mm in the resultant EPR image. Since the nitroxide spin probes we used have a triplet signal, we measured an entire spectrum with magnetic field gradients.

A compact 0.5-T MRI scanner was used to obtain 2D proton images of a phantom. The MR image was taken at Sapporo Medical University using a 0.5 T MRmini (MR Technology, Tsukuba, Japan), and data for MR imaging were acquired with software developed by MR Technology. In this study, spin-echo images of a phantom were recorded using the following parameters: TR 500 ms, TE 15 ms, FOV 38 × 38 mm, image matrix 256 × 256, NEX 4, slice thickness 3 mm, and imaging time 9 min.

3. Results

3.1. Resonance frequencies and quality factors

Key parameters for the MCPGRs were measured with and without saline solution (0.3% NaCl). This clarifies the features of the resonators used. Table 1 summarizes the quality factors and the resonance frequencies of the resonators. The resonance frequency of the MCPGR used in EPR decreased by 3 MHz when a test tube (16 mm in diameter) full of saline solution (15 ml) was placed in the

Table 1
Resonance frequencies and quality factors of MCPGRs

Sample	Resonance frequency (MHz)		Quality factor		Efficiency ($\mu T/W^{1/2}$)
	Empty	0.3% saline	Empty	0.3% saline	Empty
EPR resonator	673.5	670.5	112	103	12
NMR resonator	21.8	21.8	82	82	33

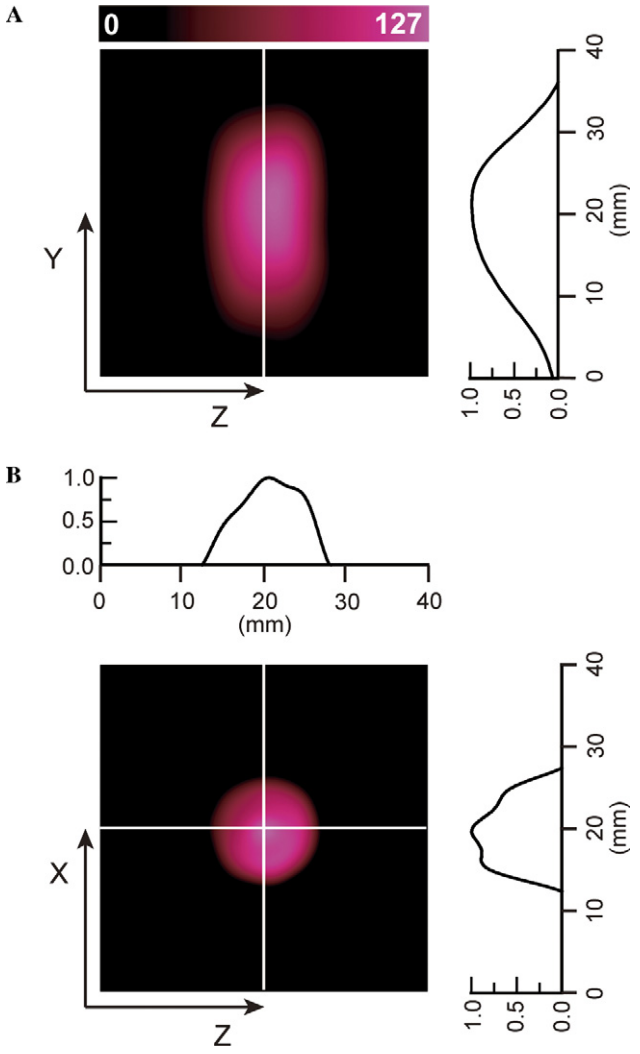

Fig. 5. 2D EPR images and intensity profiles for a test tube filled with 5 mM 4-hydroxy-TEMPO solution. (A) An EPR image in the *YZ*-plane. The parameters were as follows: magnetic field scanning 9 mT, field gradient 50 mT/m, field modulation 0.15 mT, scan time 30 s, number of projections 32, and time constant 100 ms. (B) An EPR image in the *XZ*-plane. The parameters were as follows: magnetic field scanning 8 mT, field gradient 100 mT/m, field modulation 0.15 mT, scan time 30 s, number of projections 32, and time constant 100 ms.

resonator. The quality factor of the resonator with saline solution fell to 92% of its initial value. In contrast, the quality factor of the MCPGR used in NMR was very stable even if it contained a test tube filled with saline solution. This is because the loss of the electromagnetic waves at 21.8 MHz was significantly lower than that at 670 MHz. Furthermore, the resonance frequency of the NMR resonator was not affected by saline solution.

The resonance frequency decreased by approximately 10 MHz and the quality factor increased about 10% for the MCPGR used in EPR when the MCPGR used in NMR was absent. These results show a shielding effect with the outer MCPGR. In contrast, the resonance frequency and quality factor of the MCPGR used in NMR were robust to the presence of the inner MCPGR.

3.2. RF magnetic field

The efficiency of the MCPGR used in EPR was 12 $\mu T/W^{1/2}$, and that used in NMR was 33 $\mu T/W^{1/2}$. For both resonators, the efficiencies of generating RF magnetic field were measured based on the perturbation by a metal sphere [17]. In addition to these efficiencies, we measured the image profiles in EPRI and MRI. The image profile of an obtained image depends on the distribution of the magnetic energy density in the sample, when a uniform 4-hydroxy-TEMPO solution is measured. Fig. 5 shows EPR images, in the *YZ*-plane, of 4-hydroxy-TEMPO in a test tube and normalized image profiles. In Fig. 5A, the image profile has an effective length (full width at half maximum) of 21 mm along the axis of the MCPGR. This effective length in the profile was slightly longer than the axial length (18 mm) of the MCPGR. Fig. 5B shows an EPR image of a cross-section of the test tube measured in the *XZ*-plane. The profile of the signal intensity fluctuated due to the concentration of the RF magnetic flux, and this has been called a lens effect [18]. Even if a uniform solution is measured, the EPR signal intensity cannot be homogeneous with a higher dielectric constant at ultra-high frequencies.

We also measured proton images with MRI. Fig. 6A shows a proton image of 4-hydroxy-TEMPO solution in the *YZ*-plane (38 × 38 mm) and the normalized image profile in the *Y*-direction. Since the homogeneous magnetic fields are within the region of 30 × 30 mm in our MRI scanner, we cannot obtain an appropriate image in the marginal area of the FOV. Along with the *Y*-direction, a practically uniform image was obtained in the MCPGR. Fig. 6B shows a proton image of the cross-section of the test tube with 4-hydroxy-TEMPO solution. While a uniform image profile was obtained in the *Z*-direction, a peak of the image profile near the parallel-plate capacitor was observed. As in the EPR image in Fig. 5B, an inhomogeneous magnetic field near the parallel-plate capacitor affected the image profile in MRI [19]. This was caused by the asymmetric configuration of the MCPGRs. Since the inner diameter of a measured test tube was 35% of the diameter of the MCPGR for NMR, the parallel-plate capacitor of the MCPGR for NMR was 13 mm from the test tube. In

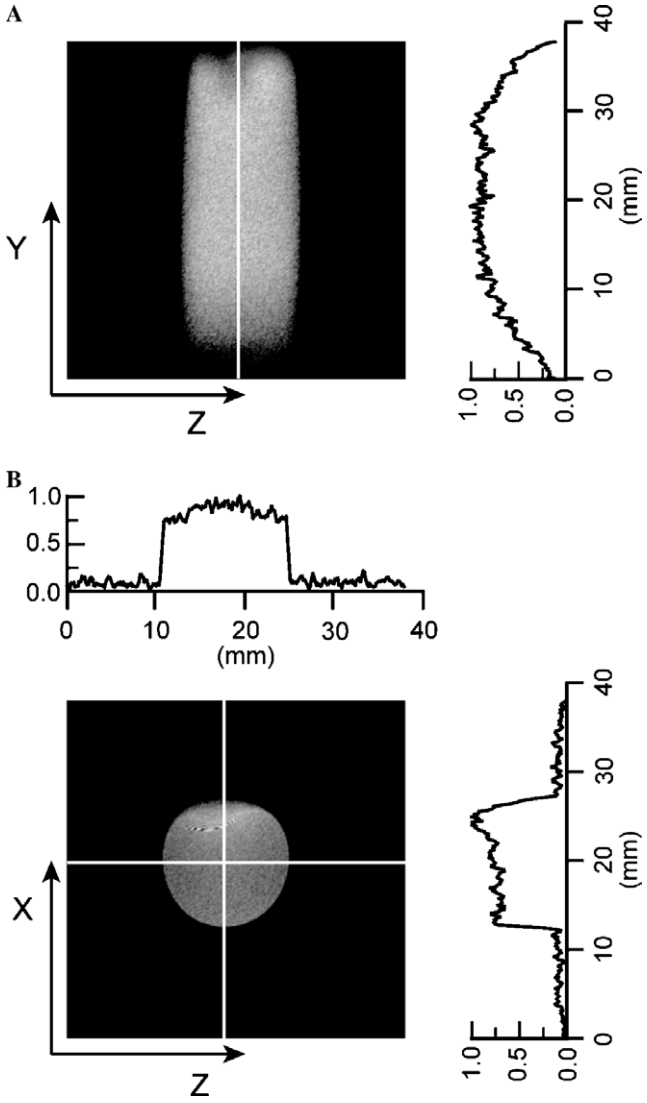

Fig. 6. 2D proton NMR images and intensity profiles for a test tube filled with 4-hydroxy-TEMPO solution. (A) An NMR image in the *YZ*-plane, and (B) an NMR image in the *XZ*-plane. For both images, the measurement parameters described in Section 2.4 were used.

contrast, the distance between the 4-hydroxy-TEMPO solution and the parallel-plate capacitor of the MCPGR for EPR was 4 mm in Fig. 6B. Thus, the parallel-plate capacitor of the MCPGR for EPR could affect the homogeneity of the RF magnetic field of the MCPGR for NMR and the image intensity.

3.3. Co-registration imaging

Images of unpaired electrons and protons were successfully obtained with the MCPGRs. Fig. 7A depicts a cross-section of the phantom. Fig. 7B shows an EPR image of the phantom, and the three tubes filled with 4-hydroxy-TEMPO solution were visualized. Since the other two tubes (distilled water) had no free radicals, those tubes were not detected in EPRI. While the FOV was set to 160 mm in data acquisition, this image (40×40 mm, 512×512 pixels) was obtained from an image of 160×160 mm (2048×2048 pixels) that was generated with the zero-filling technique. Since line-broadening occurred in 10 mM 4-hydroxy-TEMPO solution, the signal intensity was not proportional to the concentration. Thus, there was little difference between the signal intensities for 5 mM and 10 mM solution. A proton image (38×38 mm) was also acquired with the MCPGR. No significant interference due to the shielding case was observed. Fig. 7C shows five tubes, since all tubes are detectable in proton imaging. Since the relaxation time of protons is different between 4-hydroxy-TEMPO solution and distilled water, Fig. 7C shows a difference with the concentration of 4-hydroxy-TEMPO solution.

Fig. 7D shows a co-registration EPR/NMR image of a phantom. The EPR image in Fig. 7B was superimposed on the proton image in Fig. 7C by visual inspection. This result demonstrated that our application of the MCPGRs satisfies the requirements of co-registration EPR/NMR imaging mentioned in Section 2. The FOV of the NMR image was fixed in the MRI scanner we used. In contrast, the FOV of the EPR image can be adjusted by setting the magnetic field scanning and field gradient. In our experiments, although the FOVs of the two images (Figs. 7B and C) were not the same, the images could be adjusted to the actual FOVs and superimposed. We used visual inspection to superimpose the two images. While this method was easy, it was not systematic or sophisticated. However, since the main purpose of this study was to verify the concept of the composite resonator system using MCPGRs, the technical issue of automatic image alignment was beyond the scope of this investigation.

4. Discussion and conclusion

Our MCPGRs make it possible to accommodate a subject in both imaging modalities. This kind of composite resonator system should be useful in co-registration EPR/NMR imaging, since the geometry between the subject and the MCPGRs does not change due to movement from an EPR imager to an MRI scanner, and vice versa. When a unified EPR/NMR imaging instrument is available, movement between two separate imaging systems is no longer required.

The image intensity that depends on the RF magnetic field of the MCPGR was visualized with 4-hydroxy-TEMPO solution [20]. When the distribution of the RF magnetic field is changed, image profiles of a sample will be affected. While EPR image profiles in Fig. 4 do not necessarily correspond to those in an animal subject, we can easily recognize the sensitive regions of the MCPGRs in the results in Fig. 4. For the proton images in Fig. 5, these image profiles would be similar to the magnetic energy distribution in the MCPGR without a sample. This is because the RF frequency for NMR is lower than that of EPR and leads to less of a lens effect. Near the parallel-plate capacitor, less homogeneous image profiles were observed. To achieve

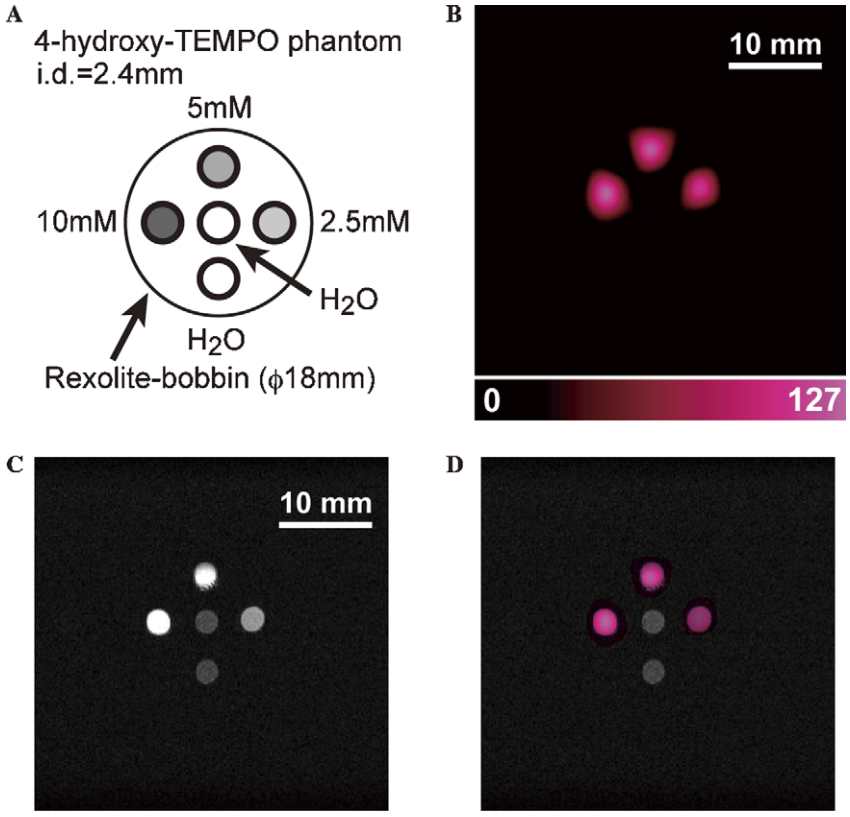

Fig. 7. (A) Capillary phantom containing distilled water and 4-hydroxy-TEMPO solution. The inner diameter of the capillary tubes was 2.4 mm. The length of the capillary tubes was approximately 60 mm. (B) EPR image of a phantom (40 × 40 mm). (C) Proton NMR image of a phantom (38 × 38 mm). (D) Co-registration EPR/NMR image.

uniform sensitivity in a subject, the RF magnetic field homogeneity must be further improved.

To improve the homogeneity of RF magnetic fields in the MCPGR used in EPR, there are two possible solutions. One is to extend the axial length of the MCPGR, which would lengthen the region of sensitivity. The other is to use more symmetric topologies for the resonators. For example, an MCPGR with two- or four-gap structures could generate a more homogeneous RF magnetic field than the MCPGR with a parallel-plate capacitor we used [21]. As well as the physical structure of the resonators, use of an MCPGR at a lower frequency decreases the lens effect due to a higher dielectric constant of the subject. Thus, it could improve the homogeneity of an RF magnetic field. The effects of eddy currents on image artifacts in an electrically conductive object have been described by Sueki and his colleagues [22]. They reported a quantitative analysis and experiments on non-uniform images in two-dimensional cw-EPR imaging. Their investigations could be helpful for improving the homogeneity of image intensity in a subject.

An inner resonator should not interfere with the electromagnetic fields of an outer resonator. In our implementation, since the MCPGR used in EPR has a resonance frequency of 670 MHz, it does not interfere with the MCPGR used in NMR at 21.8 MHz. In addition, the MCPGR interferes less with a time-varying magnetic field gradient that is perpendicular to the axis of the MCPGR. Since a conventional LGR surrounds a subject sample by cylindrical conductive elements, it may disturb a time-varying magnetic field gradient due to eddy currents in the conductive elements. Like the MCPGR, the conductivity of the sidewalls of the shielding case is crucial in MRI. If thicker conductive plates are used for the sidewalls, magnetic field gradients are not appropriately controlled due to eddy currents in the conductive plates. To avoid this problem, a printed circuit board made of epoxy resin on a fiberglass base was useful because it provided a uniform, thin, conductor as a shield.

A thin copper layer (16 μm thick) can reduce eddy currents due to magnetic field modulation as well as a time-varying magnetic field gradient. At the frequency of magnetic field modulation (90 kHz), the skin depth of copper is calculated to be 0.22 mm. Since the thickness of the copper layer is 7% of the calculated skin depth, the eddy currents generated by magnetic field modulation could be reduced. While we did not measure the eddy currents in the copper layer, the required amplitude of magnetic field modulation (0.2 mT) was obtained experimentally. While we used a uniform copper layer for a printed circuit board, a pattern of discontinuities for the conductor gives better penetration of magnetic field modulation. A theoretical

investigation of eddy currents generated due to magnetic field modulation has been reported by Mett et al. [23]. This analysis could be helpful for further improving the shielding case of the composite resonator system.

Even if a 4.7-T MRI scanner for small-animal imaging is used, its RF frequency is still 200 MHz. The difference in frequencies between NMR and EPR is 470 MHz when a 670-MHz EPR imager is used. With these frequencies and the quality factors of the resonators, strong interference between the two RF resonators is not expected. However, with a high-field MRI scanner, e.g., 9 T or higher, the RF frequencies of EPR and NMR will be close to each other. This could lead to significant coupling of the resonators. We tested the MCPGR, which has a diameter of 22 mm and a resonance frequency of near 1 GHz (data not shown) in preliminary experiments. However, the limits of the resonance frequency were not investigated. The resonance frequency depends on the parallel-plate capacitor, the inductance of individual coils, the number of coils, and the distance between individual coils. Since the MCPGR basically consists of the lumped elements, the dimensions of the elements should be shorter than the wavelength. This condition may limit the highest frequency of this configuration.

The efficiency of the MCPGR used in EPR was lower than that used in NMR, since part of the electromagnetic energy was stored in the feeding circuit that consisted of parallel transmission lines. However, a feeding circuit is useful for keeping the matching network away from the magnetic field modulation, when the matching circuit is made of varactor diodes [24]. While we did not use varactor diodes for the matching circuits of the MCPGRs, these could help to make electronically tunable functions possible. Thus, the matching network was located outside the space in the shielding case that contained the MCPGRs and a Helmholtz coil pair. This required a certain length of transmission line to feed the MCPGR used in EPR. However, further investigations are required on the relation between the length of the transmission line, the efficiency of generating the RF magnetic field, and circuit parameters in the matching network. Since the quarter-wave length coaxial lines and parallel lines are coupled with the MCPGR used in EPR, the entire RF magnetic energy is stored in both the MCPGR and the lines. This is why the efficiency of generating an RF magnetic field was decreased for the MCPGR used for EPR. The distribution of RF magnetic energy in the MCPGR and its feeding circuit can be analyzed by a method described in a report on a tunable surface-coil-type resonator for *L*-band EPR spectroscopy [25]. An approach to decreasing the stored energy in the feeding circuit could be useful for improving the efficiency of generating an RF magnetic field.

In co-registration EPR/NMR imaging, the benefits of our use of two MCPGRs are as follows: (i) RF resonators can be transferred with the subject from an EPR imager to an MRI scanner, and vice versa. This helps to avoid changes in the geometry between the subject and the RF resonators. (ii) There is less interference between the shielding case and the time-varying magnetic field gradient. (iii) The MCPGRs do not disturb the magnetic field modulation for cw-EPR detection. (iv) The two MCPGRs can be individually adjusted to the RF frequencies of EPR and NMR. The resonator system is simple and easy to implement. The MCPGRs used here are more efficient at generating an RF magnetic field than the composite resonator system previously reported [8,9,26]. The MCPGR for EPR was 2-fold more efficient than the bridged LGR used in a composite resonator; the MCPGR for NMR was 10-fold more efficient than the solenoidal coil used in a composite resonator [26]. Although He et al. reported co-registration EPR/NMR imaging with two separate instruments and two individual coils for both modalities [2], the composite resonator system reported in this article avoids the need for a specially developed sample holder to ensure position alignment for a subject.

The EPR images of each tube (Fig. 6B) are larger than their actual physical dimensions. This is because the image resolution in EPRI is less than that in MRI. A practical consideration in multimodal imaging is how to superimpose the images in different modalities while maintaining good accuracy. So far, multiple markers have been measured with a subject to adjust the position of the images of free radicals and protons. Nevertheless, markers may no longer be needed, if the geometries of the reconstructed images in both EPRI and MRI scanners are known in advance. In this approach, the relation between the subject animal and the geometry of a reconstructed image must not change. To make this possible, a composite resonator system is indispensable.

The internal diameter of the sample space was 18 mm, and the bobbin of the capillary phantom (Fig. 7A) was also 18 mm in diameter. Since the phantom just fit the sample space, the center of the phantom was kept in exactly the same position. However, rotation of the phantom was set visually. Although there could be some slight misalignment in the rotation of the phantom for EPRI and MRI, this was not necessarily a problem, since this misalignment was within the resolution of EPR imaging. Our experiments were intended to verify our concept of a composite resonator system using two MCPGRs for co-registration EPR/NMR imaging. If an EPR imager and an MRI scanner were located side-by-side or in adjacent rooms, the position of the subject animal and the composite resonator system would not be changed if it was transferred between the EPR imager and MRI scanner.

OMRI is a useful method for visualizing free radicals in a subject animal. In a recent report, ^{14}N- and ^{15}N-labeled nitroxyl radicals were simultaneously imaged by OMRI [4]. Nevertheless, EPR methods still have some advantages for investigating rich spectral information in biomedical applications. For example, spectral-spatial EPRI, a kind of functional imaging, is a useful technique in situations that involve multiple chemical species [27–30]. OMRI for animal experiments uses a lower magnetic field (approxi-

mately 15 mT for NMR detection) to avoid RF power deposition in the subject animal [4,5]. This might limit the spatial resolution of an anatomical image. In contrast, co-registration EPR/NMR imaging allows the use of a high-field MRI scanner for small-animal imaging. While EPRI currently offers less spatial resolution, a combination of a high-field MRI scanner and an EPR imager is very attractive to biomedical researchers because high-resolution anatomical images can be seen with the distribution of free radicals. When the spatial resolution of EPRI is improved, high-resolution anatomical images should be useful for investigating the distribution of free radicals in biological tissue at a smaller scale.

In conclusion, we have demonstrated the use of two MCPGRs for co-registration EPR/NMR imaging. There were no problems with interference between the resonators used in EPR and NMR. The problem regarding interference between the shielding case and time-varying magnetic field gradients was solved by using printed circuit boards made of epoxy resin on a fiberglass base. Although we have described only a co-registration image of a 4-hydroxy-TEMPO phantom, we believe that the composite resonator system with two MCPGRs reported here may be useful for co-registration EPR/NMR imaging in small animals.

Acknowledgments

The authors thank Takuro Nishiya for his assistance in early experiments and Dr. Guanglong He of the Dorothy M. Davis Heart and Lung Research Institute, Ohio State University, Columbus, OH, for a critical reading of the manuscript. We are also grateful for the discussions with Dr. George Rinard, University of Denver, Denver, CO, on MCPGR. This work was supported in part by grants from the Japan Society for the Promotion of Science (16560359, 18360194 to H.H. and 17390335 to H.F.).

References

[1] T. Sato, K. Oikawa, H. Ohya-Nishiguchi, H. Kamada, Development of an *L*-band electron spin resonance/proton nuclear magnetic resonance imaging instrument, Rev. Sci. Instrum. 68 (1997) 2076–2081.

[2] G. He, Y. Deng, H. Li, P. Kuppusamy, J.L. Zweier, EPR/NMR co-imaging for anatomic registration of free-radical images, Magn. Reson. Med. 47 (2002) 571–578.

[3] S. Matsumoto, M. Nagai, K. Yamada, F. Hyodo, K. Yasukawa, M. Muraoka, H. Hirata, M. Ono, H. Utsumi, A composite resonator assembly suitable for EPR/NMR coregistration imaging, Concepts Magn. Reson. Part B: Magn. Reson. Eng. 25B (2005) 1–11.

[4] H. Utsumi, K. Yamada, K. Ichikawa, K. Sakai, Y. Kinoshita, S. Matsumoto, M. Nagai, Simultaneous molecular imaging of redox reactions monitored by Overhauser-enhanced MRI with ^{14}N- and ^{15}N-labeled nitroxyl radicals, Proc. Natl. Acad. Sci. USA 103 (2006) 1463–1468.

[5] M.C. Krishna, S. English, K. Yamada, J. Yoo, R. Murugesan, N. Devasahayam, J.A. Cook, K. Golman, J.H. Ardenkjaer-Larsen, S. Subramanian, J.B. Mitchell, Overhauser enhanced magnetic resonance imaging for tumor oximetry: coregistration of tumor anatomy and tissue oxygen concentration, Proc. Natl. Acad. Sci. USA 99 (2002) 2216–2221.

[6] H. Li, Y. Deng, G. He, P. Kuppusamy, D.J. Lurie, J.L. Zweier, Proton electron double resonance imaging of the in vivo distribution and clearance of a triaryl methyl radical in mice, Magn. Reson. Med. 48 (2002) 530–534.

[7] W. Youngdee, D.J. Lurie, M.A. Foster, Rapid imaging of free radicals in vivo using hybrid FISP field-cycled PEDRI, Phys. Med. Biol. 47 (2002) 1091–1100.

[8] S.D. Giuseppe, G. Placidi, A. Sotgiu, New experimental apparatus for multimodal resonance imaging: initial EPRI and NMRI experimental results, Phys. Med. Biol. 46 (2001) 1003–1016.

[9] G. Placidi, M. Alecci, A. Stotgiu, First imaging results obtained with a multimodal apparatus combining low-field (35.7 mT) MRI and pulsed EPRI, Phys. Med. Biol. 47 (2002) N127–N132.

[10] S.J. McCallum, I. Nicholson, D.J. Lurie, A combined PEDRI and CW-EPR instrument for detecting free radicals in vivo, J. Magn. Reson. Ser. B 133 (1996) 65–69.

[11] S.J. McCallum, I. Nicholson, D.J. Lurie, Multimodality magnetic resonance systems for studying free radicals in vivo, Phys. Med. Biol. 43 (1998) 1857–1861.

[12] R. Murugesan, M. Afeworki, J.A. Cook, N. Devasahayam, R. Tschudin, J.B. Mitchell, S. Subramanian, M.C. Krishna, A broadband pulsed radio frequency electron paramagnetic resonance spectrometer for biological applications, Rev. Sci. Instrum. 69 (1998) 1869–1876.

[13] N. Devasahayam, S. Subramanian, R. Murugesan, J.A. Cook, M. Afeworki, R.G. Tschudin, J.B. Mitchell, M.C. Krishna, Parallel coil resonators for time-domain radiofrequency electron paramagnetic resonance imaging of biological objects, J. Magn. Reson. 142 (2000) 168–176.

[14] W.N. Hardy, L.A. Whitehead, Split-ring resonator for use in magnetic resonance from 200–2000 MHz, Rev. Sci. Instrum. 52 (1981) 213–216.

[15] W. Froncisz, J.S. Hyde, The loop-gap resonator: a new microwave lumped circuit ESR sample structure, J. Magn. Reson. 47 (1982) 515–521.

[16] H. Hirata, T. Itoh, K. Hosokawa, Y. Deng, H. Susaki, Systematic approach to cutoff frequency selection in continuous-wave electron paramagnetic resonance imaging, J. Magn. Reson. 175 (2005) 177–184.

[17] J.H. Freed, D.S. Leniart, J.S. Hyde, Theory of saturation and double resonance effects in ESR Spectra. III. rf coherence and line shapes, J. Chem. Phys. 47 (1967) 2762–2773.

[18] T. Ogata, Y. Ishikawa, M. Ono, L.J. Berliner, Visualization of eddy-current losses in *L*-band ESR imaging, J. Magn. Reson. 97 (1992) 616–622.

[19] M. Ono, A. Suenaga, H. Hirata, Experimental investigation of RF magnetic field homogeneity in a bridged loop-gap resonator, Magn. Reson. Med. 47 (2002) 415–419.

[20] G. He, S.P. Evalappan, H. Hirata, Y. Deng, S. Petryakov, P. Kuppusamy, J.L. Zweier, Mapping of the B_1 field distribution of a surface coil resonator using EPR imaging, Magn. Reson. Med. 48 (2002) 1057–1062.

[21] G.A. Rinard, G.R. Eaton, Loop-gap resonators, in: S.S. Eaton, G.R. Eaton, L.J. Berliner (Eds.), Biological Magnetic Resonance vol. 24 Biomedical EPR, Part B: Methodology, Instrumentation, and Dynamics, New York, 2005, pp. 19–52.

[22] M. Sueki, G.A. Rinard, S.S. Eaton, G.R. Eaton, Effect of eddy currents on EPR spectra, J. Magn. Reson. Ser. A 103 (1993) 208–216.

[23] R.R. Mett, J.R. Anderson, J.W. Sidabras, J.S. Hyde, Electron paramagnetic resonance field-modulation eddy-current analysis of silver-plated graphite resonators, Rev. Sci. Instrum. 76 (2005) 094702.

[24] H. Hirata, T. Walczak, H.M. Swarts, Electronically tunable surface-coil-type resonator for *L*-band EPR spectroscopy, J. Magn. Reson. 142 (2000) 159–167.

[25] H. Hirata, T. Walczak, H.M. Swarts, Characteristics of an electronically tunable surface-coil-type resonator for *L*-band electron paramagnetic resonance spectroscopy, Rev. Sci. Instrum. 72 (2001) 2839–2841.

[26] M. Alfonsetti, C.D. Vecchio, S.D. Giuseppe, G. Placidi, A. Sotgiu, A composite resonator for simultaneous NMR and EPR imaging experiments, Meas. Sci. Technol. 12 (2001) 1325–1329.

[27] S.S. Eaton, G.R. Eaton, EPR imaging, in: G.R. Eaton, S.S. Eaton, K.M. Salikhov (Eds.), Foundations of Modern EPR, Singapore, 1997, pp. 684–694.

[28] M.M. Meltempo, S.S. Eaton, G.R. Eaton, Spectral-spatial two-dimensional electron-paramagnetic-resonance imaging, J. Magn. Reson. 72 (1987) 449–455.

[29] P. Kuppusamy, M. Chzhan, K. Vij, M. Shteynbuk, D.J. Lefer, E. Giannella, J.L. Zweier, Three-dimensional spectral-spatial EPR imaging of free radicals in the heart: a technique for imaging tissue metabolism and oxygenation, Proc. Natil. Acad. Sci. USA 91 (1994) 3388–3392.

[30] H.J. Halpern, C. Yu, M. Peric, E. Barth, D.J. Grdina, B.A. Teicher, Oxmetry deep in tissues with low-frequency electron paramagnetic resonance, Proc. Natl. Acad. Sci. USA 91 (1991) 13047–13051.